Investigation of effective parameters on cladded plate delamination during pressure vessels head manufacturing by FEM and DOE

Mahmoud Afshari[1], Alireza Fallahi Arezodar[2], Iraj Sattarifar[3]

Amirkabir University of Technology (Tehran Polytechnic), Mechanical Eng. Department, 424 Hafez avenue, Tehran, Iran

Abstract

Roll-Bond cladded plates are widely used in industry. Stainless steels, Ni, Cu and Ti are used as clad usually. In multi-piece head manufacturing, while these plates press to form petals, delamination occurs in some cases. In this paper, the effective parameters on delamination are investigated. Because of more widely used in respective industry, SA 516 GR 70 as base plate and SS 316L as clad are selected. First of common criteria for defining delamination, the strain energy release rate (SERR), as explanatory parameter selected and calculated using finite element technique and VCCT method. Interface is modeled as cohesive zone with tied mesh technique and by validated experimental work. The design of experiment method is response surface methodology (RSM), and effect of input parameters on output parameter, SERR, is obtained. Results indicate that head radius have greatest impact on G and then thickness of the plate, pressing force, number of pressing steps, shear strength and friction coefficient are placed in the next rows. Among these, when the radius of the head and shear strength increase, SERR decrease and the head radius impact is much greater than shear strength. Finally, in order to prevent delamination, some strategies have been proposed.

Key Words: Roll-Bond clad plate, Delamination, VCCT, Tied Mesh method, FEM, SERR, DOE.

[1] M.afshari@aut.ac.ir
[2] Afallahi@aut.ac.ir
[3] Sattari@aut.ac.ir

Introduction

Cladded plates are widely used in the manufacture of pressure vessels (PV) and pipes. Ferrite and austenitic stainless steels, nickel base alloys, copper and its alloys and titanium, are among the materials used as clad. If using plates cladded by Roll-Bond process when forming head of PV by presses due to the low strength of the joint season, the cladded layer is separated from the base metal and delamination is happen. Therefore, in order to prevent this phenomenon, behavior of such materials under mechanical loading should be investigated.

The mechanical behavior of multilayer metals has been extensively discussed in various articles and solutions to improve their mechanical properties including flexural and fracture toughness and fatigue properties have been reported.

Lee and et. Al [1] reported that tensile strength of the multilayer sheets can be predicted by the rule of averages, However, the formability of these sheets is usually less than the amount prescribed by this rule.

Some researchers [2], [3] [4], considered these types of plates as metallic layer composites and used the equations that govern the failure of this kind of material. This assumption is also used in this article.

Tschegg and et al. [5] after 3 point bending test on specimen with crack in intermediate area Showed that both J integral and crack tip openings displacement (CTOD) decrease steadily as the crack distance approaches the intermediate region. They also showed that the substrate cracks and even the interlayer cracks had inherent asymmetry and the cracks within the softer layer are unwilling to approach the intermediate zone. According to their results, the force required to extend the interlayer crack is about half the force required to propagate the crack in each layer.

Carreno and et al. [2] examine the fracture behavior of these sheets and conclude that The crack growth in the bonding layer is not a function of the behavior of the crack movement in the adjacent layer and follows its own terms and conditions.

Sung and et. Al [6] performed tensile and bending tests on rolled bond clad plates in two heat-treated and as-rolled modes. They showed that annealing increased the ductility of the bond.

In this paper, effect of forming process parameters on delamination of cladded plates is investigated by design of experiment and finite element method. These parameters are pressing force, number of loading steps, head radius, plate thickness, friction coefficient and shear peeling strength.

The strain rate release rate criterion is considered as the criterion of separation, and then, using a validated finite element model, the effect of the process parameters is measured. Finally, the mathematical relationship between these parameters and the separation criterion is obtained and effect of each of these parameters is discussed separately.

Delamination Criteria

There are different criteria for examining crack growth in objects. In this paper, the strain energy release rate (SERR or G) criterion is used to explain delamination. The most important features of this criterion compared to other criteria are explain the brittle behavior of the bonding region, relatively simple analytic relationships, usability for anisotropic materials [7], Common for layered composite problems [8] [9] [10], and the ability to evaluate its critical value through testing on non-standard specimens with respect to the force-displacement curve area [7].

The SERR was first proposed by Griffith [11] to explain the crack growth in a completely brittle sample. According to his analysis, SERR is equal to the potential energy change, Π, in a cracked linear elastic system and nucleation and crack growth occur when the amount of this energy reaches its critical limit, G_C. In this paper, the type of loading is assumed with respect to the physics of the problem in mode II. Therefore, the relationships based on this mode have been used for the end notched flexure (ENF) specimen (Figure 1). This sample, first proposed by Russell and Street [12] , has simple geometry and clamping and computation. G_{II} values based on the initial crack length, beam theory and regardless of shear stress, are obtained from the following equations:

$$G_{II} = \frac{9P^2a^2}{16b^2h^3E_{11}} \qquad (1)$$

$$G_{II} = \frac{9a^2P\Delta}{2b(3a^3 + 2L^3)} \qquad (2)$$

In the above equations, P is the force value at the break point, Δ is the mid-point deflection of the beam, b is the sample width, h is half the beam thickness and l is the half-distance of the two supports. These equations applied to standard specimens in which the thickness and properties of the bonding region are equal to each other. Ouyang and Li [13] generalized the equation 2 for the case where the two-layer thickness and their properties differ. They found that failure mode II under pure shear loading, in fact, had very little dependence on crack length. They also show that shear bond strength is the most important parameter in determining critical load and for the same shear strength, the critical load does not increase with increasing Mod II toughness. According to their analysis, the strain release rate in Mode II will be obtained from following equation:

$$G_{II}(J/m^2) = \frac{\frac{1}{2}\left[\frac{h_1 a}{2D_1}Q_T\right]^2 + \frac{(h_1+h_2)Q_T}{2(D_1+D_2)}\delta_0}{\frac{1}{A_1} + \frac{1}{A_2} + \frac{(h_1+h_2)^2}{4(D_1+D_2)}} \qquad (3)$$

Where in

$$D_i = \frac{E_{xi} h_i^3}{12(1 - \nu_{xzi}\nu_{zxi})}$$

And

$$A_i = \frac{E_{xi} h_i}{1 - \nu_{xzi}\nu_{zxi}}$$

Index i = 1,2 represents beams 1 and 2 and A_i and D_i are axial and flexural stiffness units of beam width, respectively, under plane strain conditions. Q_T and h are reaction force of the substrate and the thickness of the layers. In this paper, Equation 3 is used to determine the critical value of G, G_{IIC} having the critical force obtained by the 3-point bending test, Fcr, and the critical relative slip value, δcr.

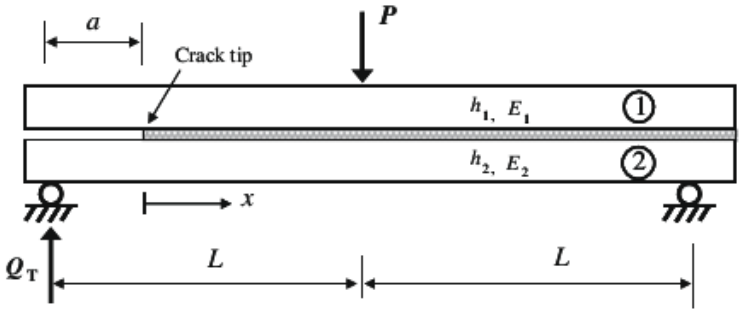

Figure 1: ENF Specimen.

Experimental procedure

In order to validate FEM model, three-point bending test was performed on the roll bonded clad plate specimen. Sample length is 150 mm, width 30 mm, thickness of clad layer and base metal are 3mm and 22 mm respectively and 15 mm crack length (fig. 2). The mechanical properties of the plate can be seen in the tables 1 and 2 based on the certificate issued by the manufacturer. The shear strength of the layers is 382 MPa and obtained from shear peeling strength test [14].

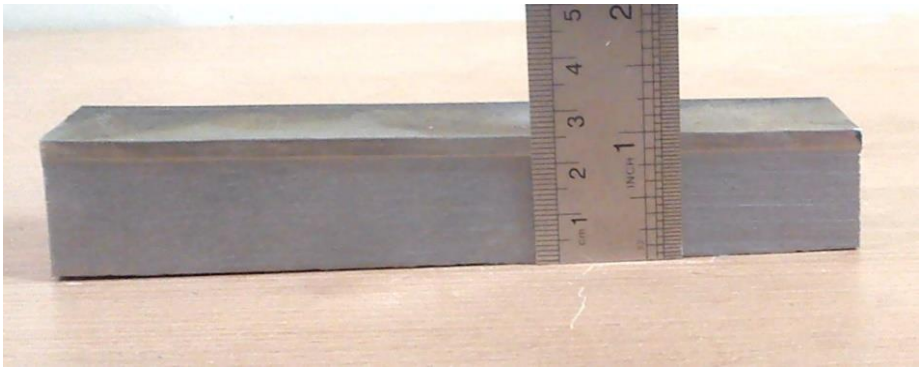

Figure 2: Roll bonded Clad plate specimen.

Table 1: SA 516 GR70 properties.

Yield stress (MPa)	U.T.S (MPa)	Elongation (%)
387.96	520.79	36

Table 2: SS 316L properties.

$R_P0.2$ (MPa)	$R_P1.0$ (MPa)	R_m (MPa)	A5 %
303	351	605	52

To create crack, first created a notch by wire cut with a 0.2mm width on one side of the sample and in the interface of the two layers. Then in order to ensure crack nucleation, specimen subjected to flexural fatigue loading under 0.2 yielding stress with frequency of 5 Hz and 60,000 cycles based on ASTM E 1820 standard. Figure 3 shows the grooves created by wire cut on the specimen.

To determine the critical value of the strain energy (G_C) by the area measurement method below the force-displacement diagram, a three-point bending loading test was performed by a Zwick device with a strain rate 5mm/min. Figure 4 shows the sample under loading.

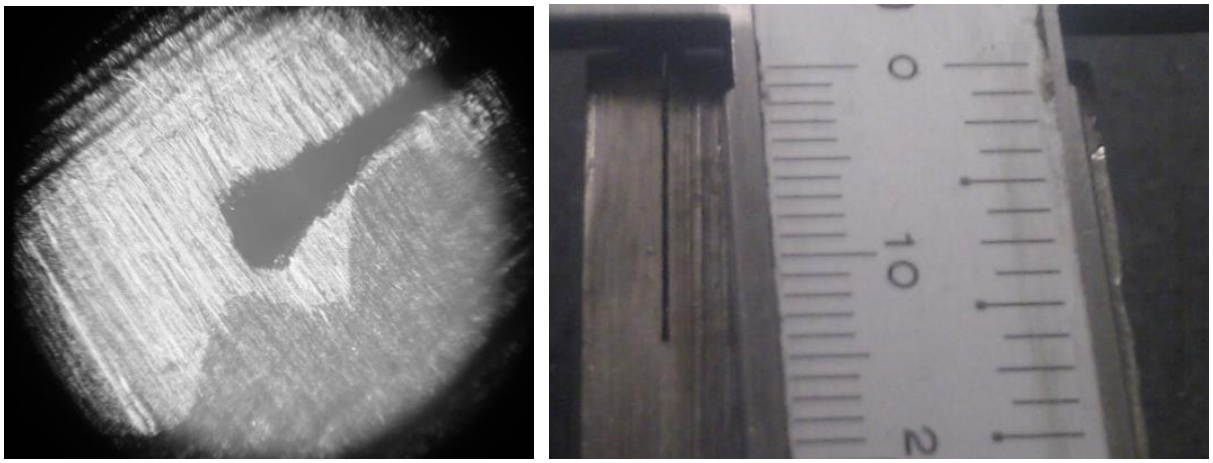

Figure 3:The notch created in clad and base plate interface on the sample edge using wire cut, 50X optical microscope image

Simulation procedure

In this paper, ABAQUS software is used to finite element modeling. In order to calculate critical SERR by FEM, virtual crack-closure technique (VCCT) is used. This method was first proposed by Rybicki and et. Al. [15]. In this technique, the value of SERR can be obtained by calculating the force and displacement of the nodes at the crack tip. For a two-dimensional model (fig. 4a) the following equation is used to calculate SERR.

$$G_{\mathrm{I}} = \frac{1}{2b\Delta a} F_{Z1}(w_2 - w_3) \qquad (4)$$

$$G_{\mathrm{II}} = \frac{1}{2b\Delta a} F_{X1}(u_2 - u_3) \qquad (5)$$

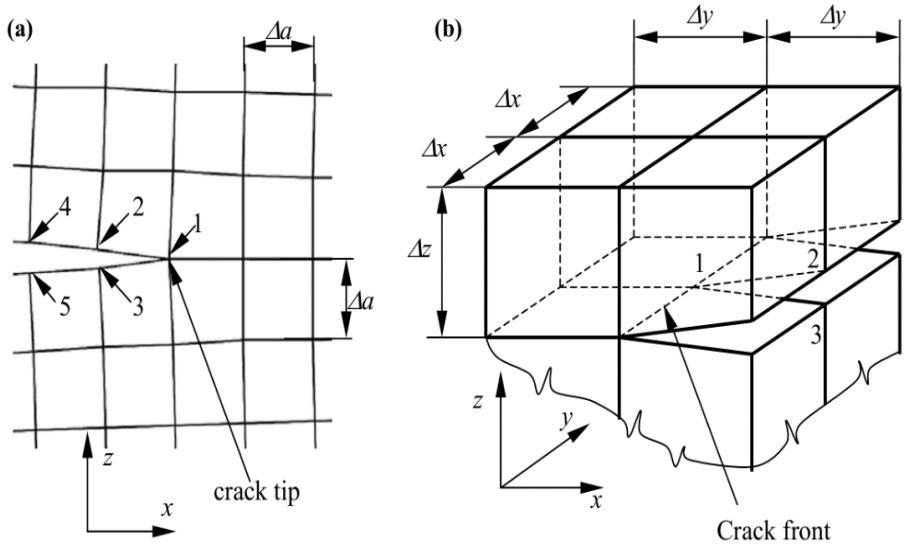

Figure **4:** Principles of VCCT.

The above equations are used to calculate the SERR value in the two-dimensional model. Therefore, specific nodes in the crack growth path are pointed in the bonding region and the amount of force applied to them and their displacement are calculated. Each of the layers and the bonding area are modeled separately. The thickness of the bonding region is considered from zero (Full Model) to 1.5 mm (Tied Mesh) in order to find its optimum value.

In the TM model, the bonding region is modeled as cohesive zone and retains its true thickness and attaches to the corresponding nodes of the surrounding layers by a movable constraint at both ends. This moving constraint preserves the equality of degrees of freedom on both sides of the bond layer and eliminates the distance between adjacent layers and greatly reduces the complexity of bond region stresses.

The material assigned to the bonding layer in the TM mode is the traction separation and the delamination mechanism is assumed quadratic. The parameter determining the node separation is maximum shear stress. The value of this stress is 382MPa obtained from the shear peeling test on clade plate according to ISO 4587 standard.

The elements of bonding layer are selected as cohesive elements, COH2D4, and their optimum size indicates the amount of crack growth, Δa, is one quarter the thickness of the bond area [16], [17]. Adjacent layer elements are linear and quadratic plane strain, CPE4I.

Material assigned to the bond layer is Traction separation and having hardness coefficients $K_{nn}=E_{11}/t$ and $K_{ns}=K_{ss}=G/t$ that t is thickness of bonding layer, G is shear modulus and equal 19.1GPa, E_{11} and E_{22} are The Young's modulus along the x and y axis respectively and are equal to the average Young's modulus of adjacent layers. E_{33} is calculated from $E=2G(1+\nu)$ and is equal to 49.66GPa. Poisson's ratio is assumed to be 0.3.

The loading is Static-General, taking into account nonlinear deformation and It has taken two steps.

In the first step the punch moves to the depth of the matrix and bends the plate, and in the second step the punch penetrates the specified amount into the plate at a defined pressure. The punch is modeled Analytical Rigid.

The force applied to the crack tip node (node 1 in Fig. 5) and the horizontal displacement of adjacent crack nodes (nodes 2 and 3 in Fig. 5) are taken as the output parameter. In order to calculate G at the starting point of crack growth by VCCT, by observing the first fall in the force-displacement diagram, the same values of force applied to node 1 and the horizontal displacement of nodes 2 and 3 are read, and by the eq. 4 and 5, the value G is calculated. As the crack grows, the node 1 at the crack tip moves element to element. Figure 6 shows the configuration and meshing of the model. Fig 7 represent the stress distribution in the crack tip.

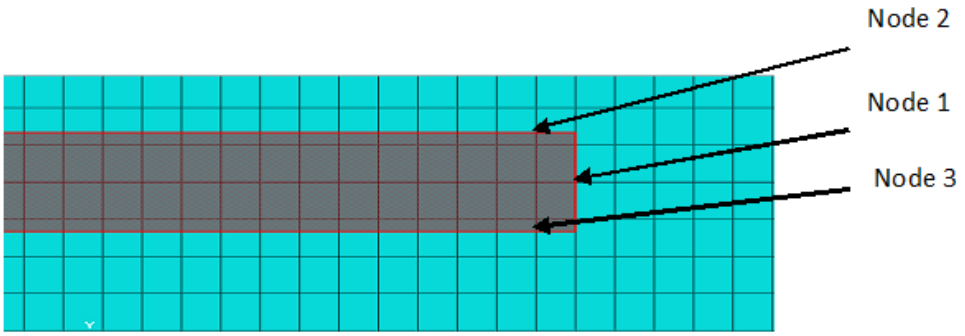

Figure 5: Meshing bonding and adjacent layers (TM with 1.5 mm thickness).

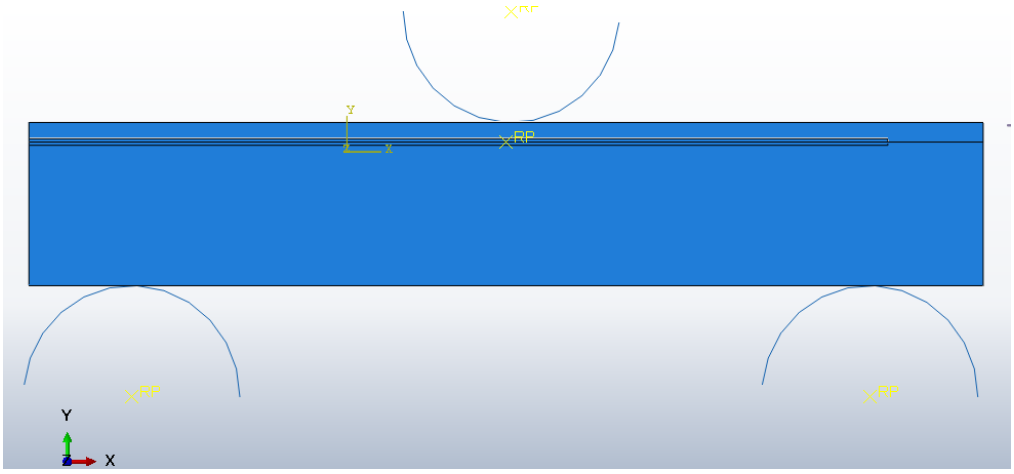

Figure 6: Configuration of the model.

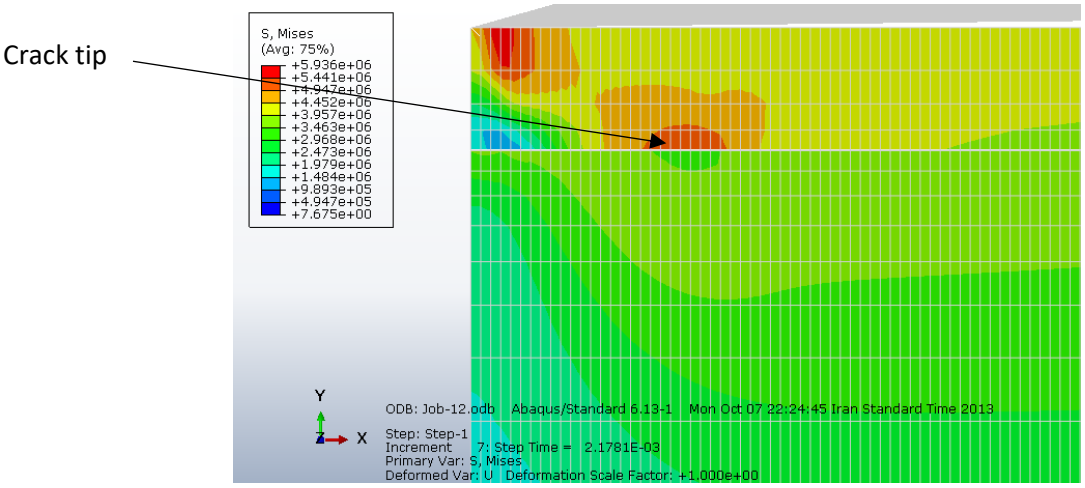

Figure 7: Stress distribution in bonding area and crack tip (thickness of bonding layer is 1mm).

Figure 8 shows the force-displacement values and Table 3 shows the G values obtained from the experimental and finite element test methods for different thicknesses. As shown, the FM model differs significantly from the experimental results. In the model with 0.25 mm thickness of bonding area (or cohesive zone), due to the excessive shrinkage of the elements and their high deformation, the Hour Glass phenomenon [18] has occurred and the analysis has not reached the starting point of crack growth. In model with 0.5 mm thickness of cohesive zone The same thing happened, but at a higher point than the previous model. In the model with 1.5mm bond region thickness, the width of the bonding element is larger than the size of the adjacent layer elements and due to their high deformation, the analysis remains incomplete. Therefore, only the FM models with zero bond thickness and the TM models with bond thicknesses of 0.75, 1 and 1.25 mm have been analyzed. The best fit to the experimental results was obtained at 2 mm thickness for the bonding elements.

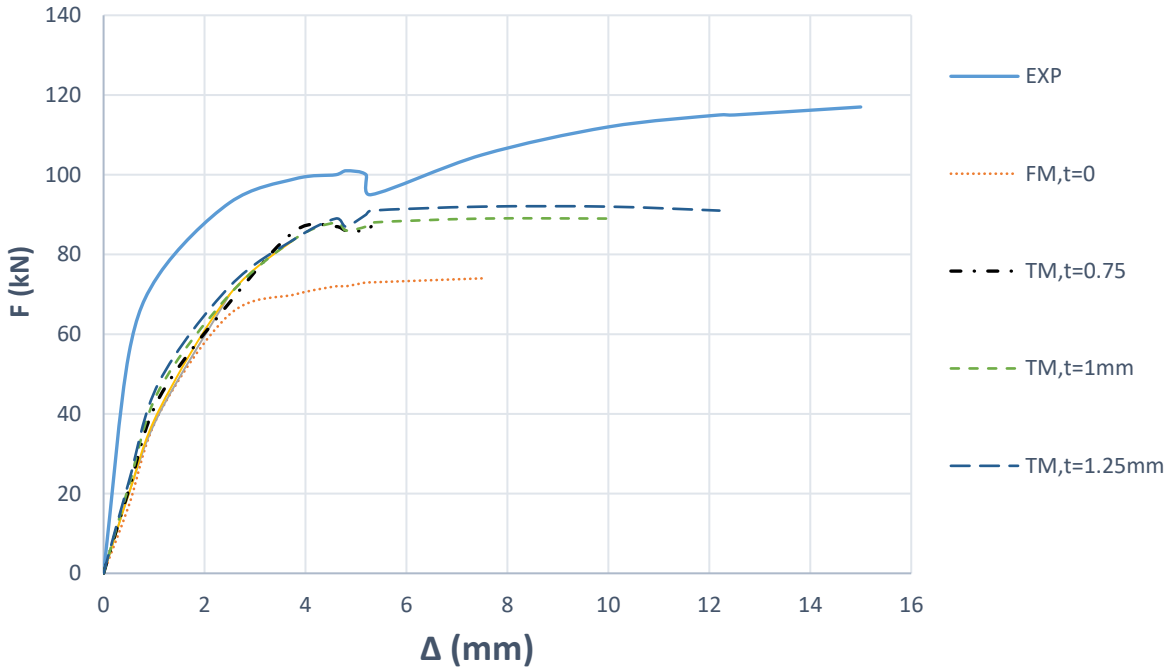

Figure 8: Numerical and experimental results.

Table **3:** Comparison of G values needed to grow interlayer crack (G_{cr}) from experimental test, Analytical solution (Ouyang and Li eq. 3) and finite element model For different thicknesses of the bonding region (t).

	The area under the curve	Ouyang and Li	t=0	t=0.75	t=1	t=1.25
G_{cr}(J/mm)	12.42	12.12	7.623	10.297	10.52	10.482
Error value (%)	-	0.9	38.6	17.12	15.29	15.6

As shown in Fig. 8, the force-displacement diagram at the breakpoint has a sudden drop and then exhibits a hardening behavior. By viewing the microscopic image of the specimen and comparing it with the crack image before bending test, this behavior of the graph can be explained by the fact that in the force drop region, some crack in the intermediate region of the two sheets has grown and because of the force required by the crack growth in the bonding region. Less than adjacent layers [2] [5], the diagram has dropped abruptly and, after some growth in the intermediate zone, the crack tends to enter the softer zone (the laminate layer) has shown a hard work behavior.

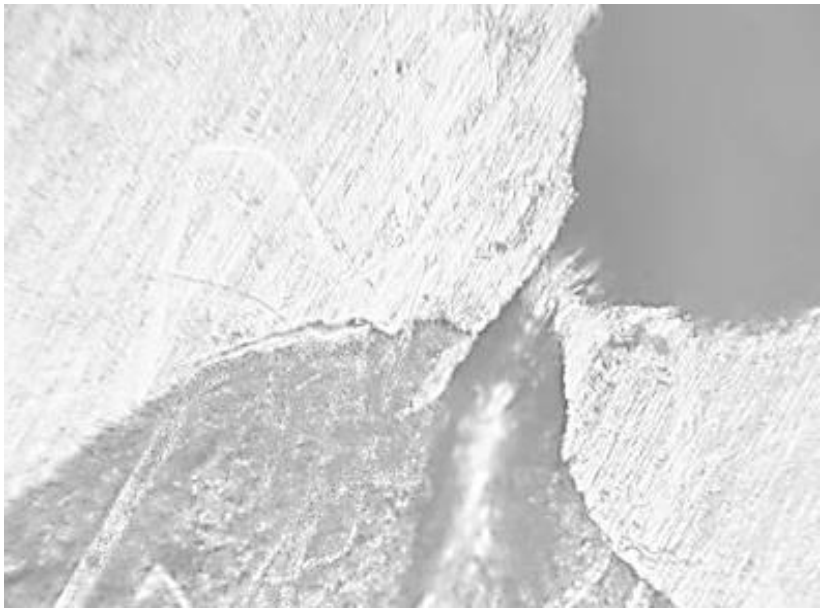

Figure 9: Crack grow after loading.

Design of Experiment

In this paper, the design of experiment (DOE) method is surface response methodology (RSM) used in 1951 by Box and Wilson [19] to improve chemical processes**.** The following general form relation shows a response level for quadratic (and first) models.

$$y = \beta_0 + \sum_{i=1}^{k} \beta_i x_i + \sum_{i=1}^{k} \beta_{ii} x_i^2 + \sum_{i<j} \sum \beta_{ij} x_i x_j + \varepsilon$$

Design Expert 7.1.1 software is used to calculate needed matrices coefficients β and drawing and output charts. The parameters studied and their values are shown in Table 4.

Table 4: Maximum and minimum values of effective parameters on delamination.

Parameter	Min	Max
Pressing force (MPa)	14 (2000psi)	35 (5000psi)
Number of loading steps	3	5
Head radius (mm)	500	4500
Plate thickness (clad +base plate)	17+3	57+3
Friction coefficient	0.1	0.3
Shear peeling strength (MPa)	120	280

Results and Discussion

After performing the analysis and before estimating the mathematical function, it is necessary to examine the significance of the effect of control variables on output. Table 5 shows the statistical summary of the data analysis. This table, which focuses on the regression-squared and predicted residual error sum of squares (PRESS), describes the status of the three linear models, the interaction effects (2F1), and the nonlinear quadratic model. Therefore, the quadratic model is proposed to estimate the effects of the parameters on the objective function because of the high value of regression coefficients and the least amount of squared error predicted.

Table **5:** Summary of Statistical Analysis of Existing Models.

Source	Std. Dev.	R-Squared	PRESS	
Linear	27.93	0.162	0.0299	
2F1	31.25	0.511	0.0543	
Quadratic	17.21	0.69	0.0214	**Suggested**

Table 6 shows the values of the experimental design input parameters and the results obtained. Finally, the following equation is obtained that shows the effect of input parameters on the strain Energy Release Rate.

Table 6: values of the experimental design input parameters and the results obtained

	A	**B**	**C**	**D**	**E**	**F**	**Result**
Run number	Pressing force (MPa)	Head radius (mm)	Plate thickness (mm)	Friction coefficient	Shear strength (MPa)	Number of loading steps	**G_{II} (KJ/mm)**
1	35	4500	40	0.1	280	3	**0.0164**
2	14	4500	20	0.1	280	5	**0.0239**
3	35	500	60	0.3	280	3	**53.63**
4	14	4500	60	0.1	280	3	**2.8488**
5	35	500	60	0.3	280	5	**48.88**
6	24.5	4500	60	0.3	280	3	**3.017**
7	24.5	2500	20	0.2	200	3	**0.3835**
8	35	4500	60	0.3	200	3	**7.33**
9	24.5	500	20	0.3	120	5	**34.21**
10	35	500	60	0.1	280	5	**49.12**
11	14	2500	40	0.2	200	5	**1.591**
12	24.5	500	60	0.1	120	3	**19.476**
13	35	500	20	0.1	120	3	**40.49**
14	24.5	4500	60	0.3	280	5	**1.714**
15	14	500	20	0.3	280	4	**19.08**
16	14	2500	60	0.3	280	3	**0.153**
17	35	4500	20	0.3	120	3	**0.2511**
18	35	4500	20	0.3	280	5	**0.00302**
19	14	4500	20	0.2	280	3	**0.00106**
20	14	500	20	0.1	120	5	**33.61**

21	24.5	500	20	0.1	280	4	**17.42**
22	35	4500	20	0.3	120	5	**0.00375**
23	35	500	40	0.1	120	5	**29.1**
24	14	500	60	0.1	200	5	**38.81**
25	14	4500	20	0.3	200	4	**0.00308**
26	14	4500	60	0.1	120	5	**2.477**
27	29.75	2500	50	0.15	160	3	**13.583**
28	24.5	4500	20	0.1	120	3	**0.245**
29	35	500	20	0.3	200	5	**26.59**
30	35	4500	60	0.1	200	5	**2.209**
31	14	500	60	0.3	200	4	**49.64**
32	14	500	40	0.1	280	3	**13.88**
33	35	4500	20	0.1	200	5	**0.00127**
34	35	2500	60	0.3	120	3	**0.359**
35	14	4500	60	0.2	120	3	**1.367**
36	35	500	40	0.1	120	4	**14.02**
37	35	2500	60	0.3	120	5	**0.479**
38	24.5	500	60	0.3	120	3	**33.07**
39	14	4500	20	0.3	200	5	**0.000889**
40	35	500	20	0.3	200	3	**24.6**
41	14	500	20	0.3	280	5	**19.088**
42	35	500	20	0.2	280	5	**19.72**
43	14	500	20	0.3	120	3	**40.683**

$$G(J/mm) = -183.6 + 126.41 \times A - 1579.43 \times B + 373.85 \times C + 47.45 \times D - 57.20 \times E - 80.83 \times F$$
$$-1.37 \times AB + 101.48 \times AC - 52.81 \times AD + 300.13 \times AE - 223.06 \times AF - 315.78 \times BC$$
$$-175.14 \times BD + 160.11 \times BE - 28.73 \times BF + 77.6 \times CD + 581.31 \times CE + 99.95 \times CF \quad (6)$$
$$-84.09 \times DE - 2.57 \times DF - 74.51 \times EF + 441.38 \times A^2 + 1452.43 \times B^2$$
$$+830.41 \times C^2 - 763.30 \times D^2 + 9.14 \times E^2 + \varepsilon$$

That A, B, C, D, E and F Are Press in Mpa, head radius, plate thickness, friction coefficient, shear strength in MP and number of press steps respectively. Also ε is the error value or noise of the results. As shown in equation 6, the head radius has the greatest effect on G_{II}, followed by plate thickness, pressing force, number of pressing steps, shear strength of the sheet, and friction coefficient.

Figure 10 shows the effect of increasing the radius and thickness on the value of G. As can be seen, increasing the head radius reduces the deformation in the intermediate region, thereby reducing G. Increasing the thickness of the plate increases the G and consequently increases the probability of delamination. As the bond layer distance from the neutral axis of the plate is increased and its deformation is increased by bending and the stress in this area increases sharply.

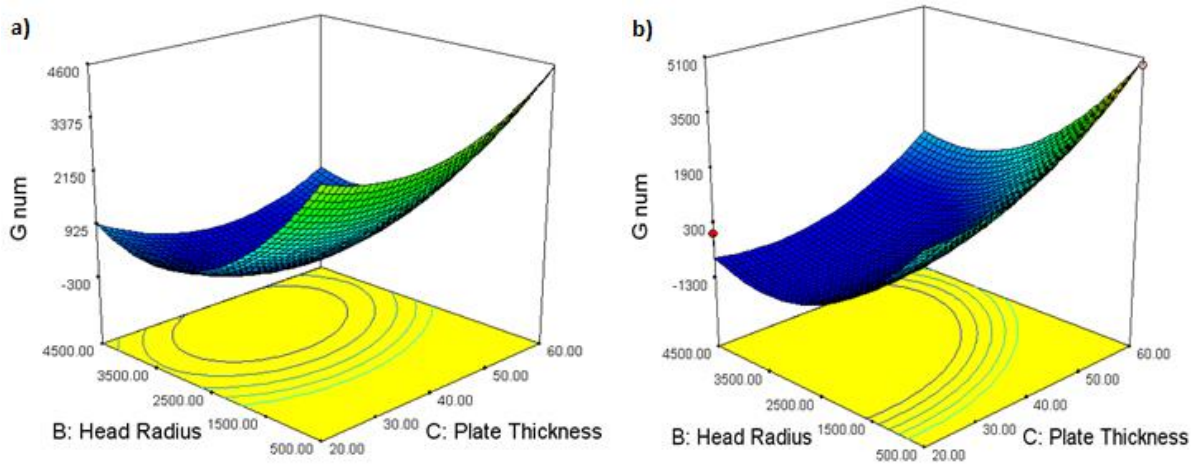

Figure 10: Effect of increasing radius and thickness on G, a) other parameters in minimum and b) other parameters in maximum value.

The next influential parameter is the punch pressure, which increases with increasing G. As can be seen in Figure 11. If the punch pressure increase, the strain on the xy plane of the bond plate also increases, which increases the stress in this area. As result, the strain energy will reach its critical value faster.

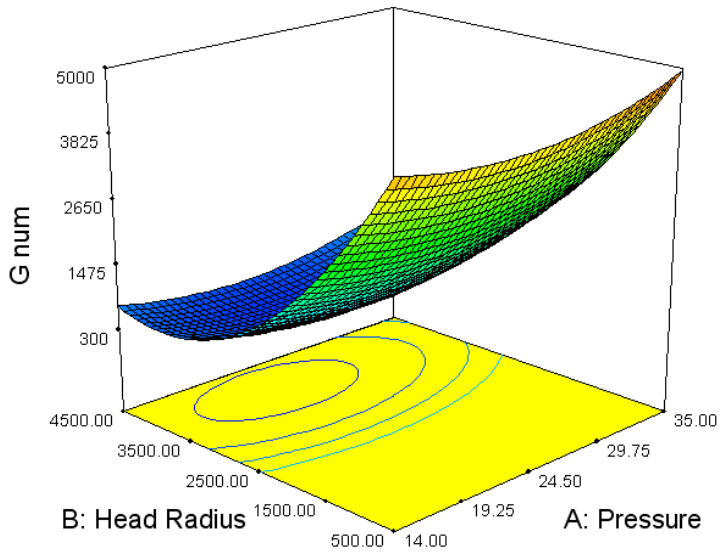

Figure 6: effect of punch Pressure and head radius on G, Other Parameters are in intermediate level.

Fig. 12 shows that the effect of pressure on G, depend on the amount of shear strength. While number of forming steps is high (or depth of penetration is low), if there is low shear strength, increasing pressure decrease G. This is because the increase in forming pressure prevent the sliding of the layers in the bonding area relative to each other due to friction between them. According to Russell and Street report [12] friction between crack surfaces absorbs some fracture energy. Gillespie and et al. [20] obtained amount of this energy reduction for the ENF sample by finite element. They concluded that the friction between the two crack surfaces absorbs 2 to 4 percent of the fracture energy. Increasing pressure increases the friction effect and thereby increases the amount of energy absorbed. This is particularly noticeable in high-thickness plates that require a large number of forming steps.

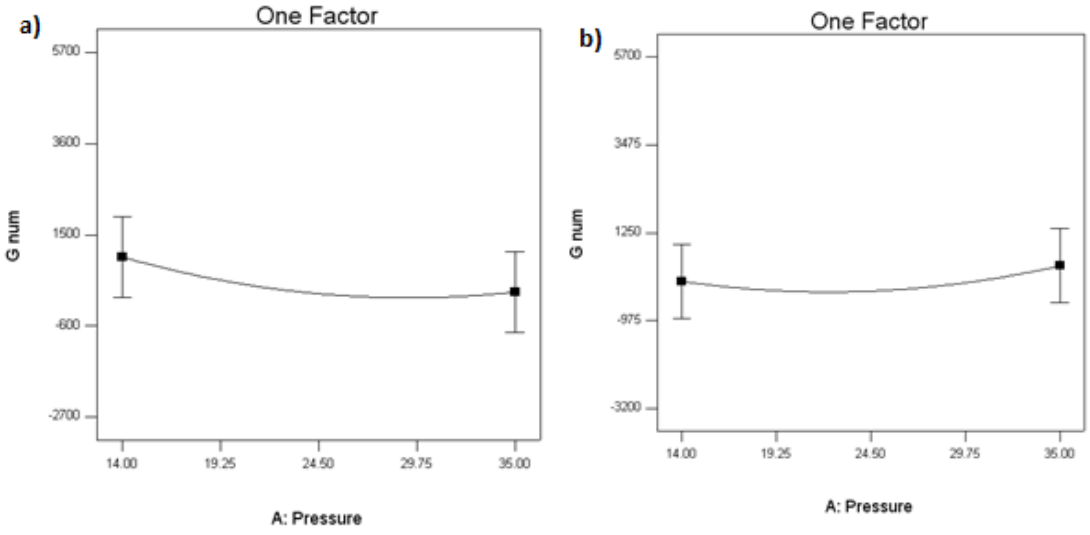

Figure 12: Effect of increasing pressure on G. Number of pressing steps is 5 and other parameters are in intermediate level. Shear strength is a) 120 Mpa and b) 280Mpa.

Fig. 13 shows effect of thickness and radius on delamination. While forming in 5 steps, G values are less dependent on thickness and radius. The exact number of forming steps is determined when the critical value of the fracture energy, G_{IIC}, is obtained by testing the specimen prepared from the plate. In this figure the blue area is a safe area of formation.

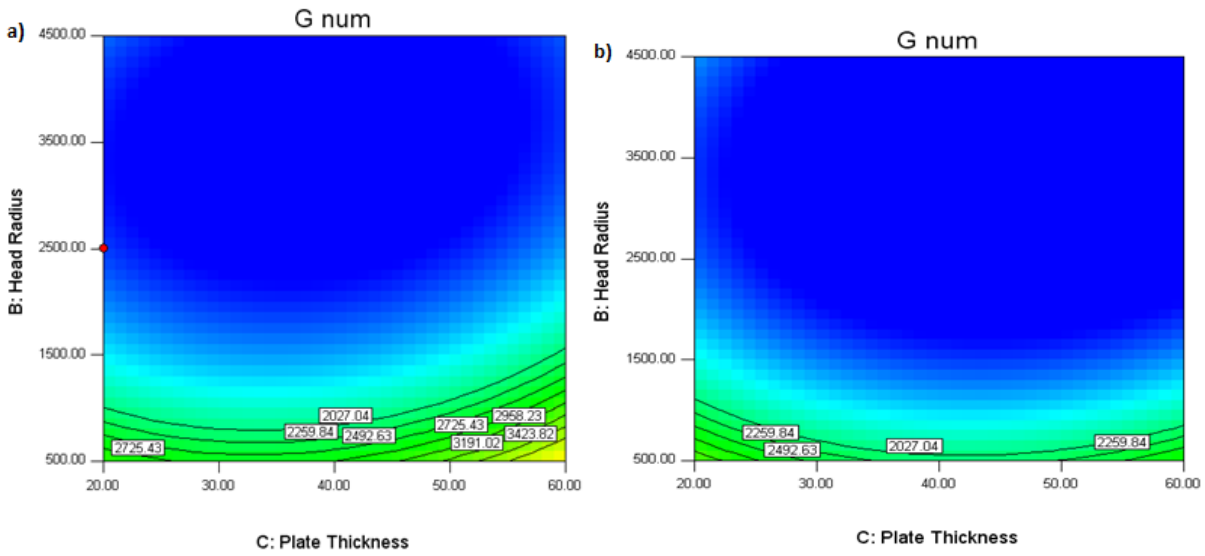

Figure 7: Effect of thickness and radius on delamination, Number of pressing steps in a) is 3 and in b) is 5, other parameters are in intermediate level.

Fig. 14 show effect of plate thickness on G. According to the equation 6 the interaction of thickness and shear strength has the greatest effect on G value. As can be seen, if the penetration depth in each step is high (the number of steps is low) and the shear strength of the sheet is low, increasing the sheet thickness will decrease G. In this case (high thickness and low shear strength) changes in the parameters that reduce the relative slip of adjacent layers at the bonding surface of the two sheets will decrease the G. These include increasing pressure and reducing the number of pressing steps.

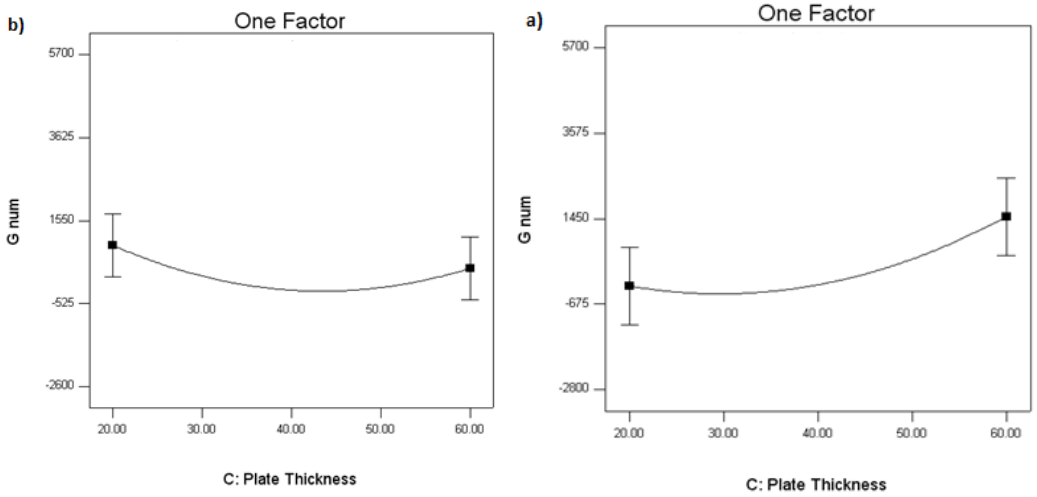

Figure **8:** The effect of increasing thickness on G, forming in 3 steps, a) Peeling shear strength in a) is 280 Mpa and in b) 120 Mpa.

Conclusion and some offers to avoid delamination

In order to determine the critical fracture toughness, a specimen is prepared from the plate and the G_{IIC} value is measured by peeling shear test. Then by putting the effective parameters such as thickness, radius, and shear strength in eq. 6, the G value is calculated and compared with the G_{IIC} value of the test.

- If this value is higher than the G_{IIC}, the plate will delaminate probably under these conditions. If this value is very close to G_{IIC}, delamination can be prevented by changing the less effective parameters such as decreasing the friction coefficient and increasing the number of pressing steps.
- If the plate thickness is high, the change in shear strength of the sheet will not have much effect on the delamination, and heat treatment to increase bond strength prior to forming will be a waste of time and cost.
- According to objective observations, for forming radius of 500mm or less, plates coated by explosive welding also sometimes have interlayer detachment. Therefore, for radii below this value, the base plate is first formed and then the coating layer is created by Submerged arc welding with a strip electrode on the base metal and, if necessary, the surface is machined or grinded.
- According to the results, if the shear strength of the sheet is low, increasing the pressing pressure will reduce the probability of interlayer separation. This is particularly noticeable in high-thickness plates that require a large number of forming steps. In these cases, the relative sliding of the layers should be avoided. For this purpose, the penetration depth and pressure of the forming can be increased.
- In case of Submerged arc welding or thermal spraying if temperature rise is problematic and the plate cannot be coated in this way, stress relieving operation should be performed between the plate forming steps.

Declarations

Not applicable.

References

[1] Lee S.; Wadsworth J.; Sherby OD.;, "Tensile properties of laminated composites based on ultrahigh carbon steel," *Compos Mater,* vol. 25, pp. 842-53, 1991.

[2] Carreno F; Chao J; Pozuelo M; Ruano OA;, "Microstructure and fracture properties of an ultrahigh carbon steel-mild steel laminated composite," *Scripta Mater,* vol. 1135, pp. 40-48, 2003.

[3] Pozuelo M; Carreno F; Caesi M; Ruano OA, "Influence of interfaces on the mechanical properties of ultrahigh carbon steel multilayer laminates," *Int J, Mater Res,* vol. 98, pp. 47-52, 2007.

[4] Nambu S.; Michiuchi M.; Inoue J.; Koseki T, "Effect of interfacial bonding strength on tensile ductility of multilayered steel composites," *Composites Science and Technology,* vol. 69, p. 1936–1941, 2009.

[5] E.Tschegg; H.O.K.Kirchner and M. Kocak, "Cracks At The Ferrite-Austenite Interface," *Acta metall, mater,* vol. 3, pp. 469-487, 1990.

[6] Sung-Tae Hong K.; Scott Weil;, "Niobium-clad 304L stainless steel PEMFC bipolar," *Journal of Power Sources,* vol. 168, pp. 408-41, 2007.

[7] T.L.Anderson, Fracture Mechanics: Fundamentals And Application, Third Edition, Taylor and Francis CRC press, 2005.

[8] Wang J.; Qiao P, "On the energy release rate and mode mix of delaminated shear deformable composite plates," *International Journal of Solids and Structures,* vol. 41, pp. 2757-2779, 2004.

[9] AndrásSzekrényes, "Interlaminar stresses and energy release rates in delaminated orthotropic composite plates," *International Journal of Solids and Structures,* vol. 49, no. 18, pp. 2460-2470, 2012.

[10] AndrásSzekrényes, William MartinsVicente, "Interlaminar fracture analysis in the GII–GIII plane using prestressed transparent composite beams," *Composites Part A: Applied Science and Manufacturing,* vol. 43, no. 1, pp. 95-103, 2012.

[11] G. A. A., "The phenomena of rupture and flow in solids," *Philosophical Transactions of the Royal Society of London, Series A, Containing Papers of a Mathematical or Physical Character,* pp. 163-198, 1921.

[12] Russell A. J. & Street K. N., "Moisture and temperature effects on the mixed-mode delamination fracture of unidirectional graphite/epoxy. Delamination and debonding of materials," *ASTM, STP,* p. 876, 1989.

[13] Zhenyu Ouyang; Guoqiang Li;, "Nonlinear interface shear fracture of end notched flexure specimens," *International Journal of Solids and Structures,* vol. 46, pp. 2659-2668, 2009.

[14] *ASTM A264.*

[15] E. F. Rybicki and M. F. Kanninen;, "A Finite Element Calculation of Stress Intensity Factors by a Modified Crack Closure Integral," *Eng. Fracture Mech,* vol. 9, pp. 931-938, 1977.

[16] AndreaSpaggiari, EugenioDragoni, Hal F.Brinson, "Measuring the shear strength of structural adhesives with bonded beams under antisymmetric bending," *International Journal of Adhesion and Adhesives,* vol. 67, pp. 112-120, 2016.

[17] ZoltánJuhász, AndrásSzekrényes, "The effect of delamination on the critical buckling force of composite plates: Experiment and simulation," *Composite Structures,* vol. 168, pp. 456-464, 2017.

[18] *Abaqus 6.8 documentation, part 3, Mesh module, Understanding adaptive remeshing.* [Performance].

[19] G.E.P. Box, K.B. Wilson, "On The Experimental Attainment of Optimum Conditions," *G.E.P. Box, K.B. Wilson, "On The Experimental Attainment of Optimum Conditions" J. of the Royal Statistical Society. Series B 13. P.1–45, 1951.,* vol. Series B13, pp. 1-45, 1951.

[20] Gillespie, J. W.; Carlsson, L. A.; Pipes, R. B.; Rothschilds R.; Trethewey; B. and Smiley A.;, "Delamination growth in composite materials final report," NASA-CR-176416, 1985.

[21] S. P.S, "Bimaterial interface instabilities in plastic solids," *Int J Solids Struct,* vol. 22(2), p. 195–207, 1986.

[22] Inoue J; Nambu S; Ishimoto Y; Koseki T, "Fracture elongation of brittle/ductile multilayered steel composites with a strong interface," *Scripta Mater,* pp. 105-109, 2008.

[23] R. H. Martin, "corporating interlaminar fracture mechanics into design", Intern," in *tional Conference on Designing* , London, UK, 1998.

[24] Carlsson, L. A.; Gillespie J. W. & Pipes, R. B.;, "On the analysis and design of the end notched flexure (ENF) specimen for mode II testing," *J. Composite Mater,* vol. 20, pp. 594-604, 1986.